

*Original Research*

# Optimization of The Modified Soybean Straw Activated Carbon for Adsorption of Methylene Blue Dye by Response Surface Methodology

Rurong Jiang<sup>1\*</sup>, Jinhua Yao<sup>1</sup>, Yonglian Yao<sup>2</sup>

<sup>1</sup>School of Public Utilities, Jiangsu Urban and Rural Construction Vocational College, Changzhou 213247, China

<sup>2</sup>CAUPD Beijing Planning & Design Consultants Company, Beijing, 100044, China

*Received: 17 April 2023*

*Accepted: 20 May 2023*

## Abstract

A low-cost modified soybean straw activated carbon (M-SSAC) adsorbent was prepared from soybean straw for the methylene blue (MB) adsorption from dye wastewater. The effects of pH, adsorbent dosage, initial MB concentration, and adsorption time on the adsorption of MB were investigated by response surface methodology (RSM), and the experimental conditions were optimized. The results showed that the adsorbent dosage had the most significant effect on the adsorption capacity of MB adsorbed by M-SSAC. The best adsorption effect was achieved at pH 6.6, an adsorbent dosage of 0.05 g, an initial MB concentration of 190 mg/L, and an adsorption time of 110 min, with an average adsorption capacity of 41.96 mg/g and an error of 1.19% from the predicted value. This result indicated that the optimized adsorption conditions based on the response surface method are accurate and reliable. Compared with the Freundlich model, the Langmuir model was more suitable for modeling the adsorption of MB by the M-SSAC. The adsorption process was consistent with Pseudo-second-order kinetics, and the thermodynamic calculations showed that the adsorption process was a spontaneous heat absorption process. The results suggest that M-SSAC is a promising adsorbent for effectively removing MB dye from wastewater.

**Keywords:** adsorption, optimization, methylene blue (MB), modified soybean straw activated carbon (M-SSAC), response surface methodology (RSM)

## Introduction

Methylene blue (MB) is a cationic dye of phenothiazine salt widely used as a chemical indicator, dye, biological stain, and drug manufacturing [1, 2].

In developing countries, the production of dyestuffs is steadily increasing every year. The textile, pharmaceutical, leather, food processing, cosmetic and coating industries discharge more than 800,000t of various dyestuff wastewater annually, accounting for about 10% to 15% of the total [3]. Without proper treatment, these toxic, mutagenic, and carcinogenic dyes can harm the environment and marine life and seriously threaten human health [4, 5]. For example,

---

\*e-mail: 010278@jsgcc.edu.cn

the accumulation of MB in wastewater can cause adverse effects on human health, such as breathing difficulties, vomiting, eye burns, diarrhea, and nausea [6]. Therefore, removing dyes from wastewater is essential to protect the environment and human health.

Dye wastewater is usually treated by physical and chemical methods such as membrane filtration, photocatalytic degradation, flocculation, oxidation, biological treatment, and conventional adsorption [7-10]. Adsorption is a method of using porous solids to adsorb some or several pollutants in sewage to recover or remove these pollutants so that the sewage can be purified. Among many dye wastewater treatment technologies, adsorption is considered one of the best treatment methods due to its good treatment effect, ease of operation, and high recoverability [11, 12].

Biomass adsorbent is a vital material widely used in chemical separation, industrial adsorption, wastewater treatment, and soil remediation. Its preparation of raw materials is mainly based on agricultural and forestry solid waste, which is of great importance for protecting the environment and saving resources [13, 14]. China has a wide soybean cultivation area and abundant soybean straw resources. As an agricultural waste, soybean straw contains about 48.7% cellulose, 12.7% hemicellulose, 27.12%~36.98 % lignin, and 2.90% ash [15]. Cellulose and hemicellulose contain mainly oxygen-containing functional groups, such as carboxyl, hydroxyl, ether, and carbonyl [16]. Lignin is a highly polymerized phenolic polymer with reactive groups such as aromatic groups, phenolic hydroxyl groups, and conjugated double bonds in the molecular structure [17]. Soybean straw has the advantages of high fixed carbon content, volatile components, and low ash content with a well-developed honeycomb pore structure with strong adsorption properties. Soybean straw is easy to be modified and chemically modified, making it an excellent raw material for the preparation of adsorbents [18]. Miao et al. studied the removal of phenol by soybean straw, the results showed that the maximum monolayer adsorption capacity of phenol achieved 278 mg/g, and the value of  $R_L$  was found to be below 1.0, indicating that the soybean straw activated carbon was favorable for phenol adsorption [19].

Therefore, this paper prepared modified soybean straw activated carbon (M-SSAC) by charring in a muffle furnace with sodium hypochlorite and ultrasonic activation using soybean straw as raw material. The effects of solution pH, adsorbent dosage, initial MB concentration, and adsorption time on the adsorption value of MB were investigated by Box-Behnken Design in response surface method (RSM), and the optimized preparation conditions were obtained. The adsorption isotherm, adsorption kinetics, and adsorption thermodynamics were used to analyze the adsorption process of M-SSAC on MB under the optimized conditions to provide some reference for improving the utilization of soybean straw and MB wastewater treatment.

## Materials and Methods

### Preparation and Activation of Adsorbent

The soybean straw used in this study was purchased from Heze City, Shandong Province. Before use, the soybean straw was washed five times with tap water to remove impurities, and then the soybean straw was rinsed thoroughly with distilled water and dried at 105°C for 24 h until constant weight. Weigh 30 g of sieved soybean straw into a tube furnace and pass nitrogen as a protective gas for charring, holding at 500°C for 60 min, controlling the temperature increase rate of 5°C/min. Will well-charred charcoal powder into a beaker, add a concentration of 1 mol/L of sodium hypochlorite 100 mL, ultrasonic acid leaching for 40 min, and finally washed with distilled water to pH 7. The washed soybean straw was dried at 105°C for 24 h until constant weight. Finally, the dried soybean straw was crushed, and sieved with a 200 mesh sieve to obtain a particle size of about 75  $\mu\text{m}$  modified soybean straw powder.

### RSM Design

The experiments were conducted using DesignExpert 8.0.6 for the Box-Behnken Design of RSM. The four influencing factors: solution pH (5.5~7.5), adsorbent dosage (0.05~0.15 g), initial MB concentration (100~200 mg/L), and adsorption time (20~100 min) were selected as independent variables for a four-factors, three-levels response surface analysis test. A quadratic regression was performed with the adsorption capacity of MB as the response value to obtain the optimized adsorption conditions. The influencing factors and values are shown in Table 1.

### Adsorption Isotherm Test

A series of 50 mL conical flasks were filled with 25 mL of MB solutions at concentrations of 20 mg/L, 60 mg/L, 100 mg/L, 150 mg/L, 200 mg/L, 250 mg/L, 300 mg/L, and 400 mg/L, respectively. The 0.05 g of M-SSAC was added at three temperatures of 288, 298 K and 308 K, respectively, in a water bath shaker at 120 r/min for an adsorption isotherm study.

Table 1. Experimental factors and levels.

Factors		Levels		
		-1	0	+1
A	pH	5.5	6.5	7.5
B	Adsorbent dosage (g)	0.05	0.10	0.15
C	Initial MB concentration (mg/L)	100	150	200
D	Adsorption time (min)	20	70	120

### Adsorption Kinetic Test

A series of 50 mL conical flasks were filled with 25 mL of MB solution at a concentration of 200 mg/L, followed by 0.05 g of soybean straw, and shaken at 120 r/min in a water bath shaker at 25°C. Samples were taken at 5, 10, 20, 30, 50, 70, 90, 120, 150, 180, and 240 min for the adsorption kinetics study, respectively.

### Analysis Method

The concentration of MB was determined using a UV-VIS spectrophotometer (DR3900, Hach, USA) at a maximum wavelength of 470 nm. Design Expert 8.0.6 and origin 2022 were used for experimental design, parameter determination of regression equations, and response surface plotting.

### Calculation

In this experiment, the adsorption performance of M-SSAC was evaluated using the adsorption capacity of MB as an index. After the adsorption experiment, the conical flask was quickly removed and passed through a 0.45 μm filter membrane. The absorbance was measured at 470 nm with a UV-VIS spectrophotometer. The remaining concentration of MB was calculated from the standard curve to calculate the adsorption amount  $q_t$  with the following Eq. (1):

$$q_t = \frac{(C_0 - C_t)V}{m} \quad (1)$$

Where  $q_t$  is the amount of MB adsorbed at moment  $t$ , mg/g;  $C_0$  is the initial concentration of MB solution, mg/L;  $C_t$  is the concentration of MB at moment  $t$ , mg/L;  $V$  is the volume of MB solution, L;  $m$  is the mass of M-SSAC, g.

## Results and Discussion

### Optimization of Adsorption Conditions

#### *Response Surface Model and Significance Test*

The response surface experimental design and the results of the response values are shown in Table 2. To investigate the effects of pH, adsorbent dosage, initial MB concentration, and adsorption time on the removal of MB by the M-SSAC, the data were subjected to multiple regression analysis using Design Expert. The fitted model results were subjected to ANOVA, while significance tests were conducted for each factor using F values. The resulting multiple quadratic regression equation is shown in Eq. (2).

$$Y = 32.58 + 2.90A - 4.17B + 2.89C + 2.42D + 0.25AB - 0.094AC - 0.40AD - 0.29BC + 0.071BD + 0.26CD - 8.64A^2 + 0.53B^2 + 0.77C^2 + 0.43D^2 \quad (2)$$

The positive coefficients of variables A, C, and D in Eq. (2) indicated that they all caused an increase in the response value, and the negative coefficients of variable B indicated that it caused a decrease in the response value. The model regression results showed that the F value was 190.91, and the signal-to-noise ratio was 30.33, which was much higher than 5, indicating that this regression model was significant. The  $R^2$  and adj  $R^2$  of Eq. (2) were 0.9944 and 0.9892, with  $p < 0.0001$ , indicating that the empirical model could better reflect the experimental data and the experimental error was small, and the adsorption test conditions could be optimized.

As shown in Table 3, the effects of A, B, C, D, and  $A^2$  on Y values were significant ( $p < 0.0001$ ), the effects of pH, adsorbent dosage, initial MB concentration, adsorption time, and the square of adsorbent dosage were significant. In contrast, the effects of other influencing factors were not significant. In addition, the sum of squares of different influencing factors in Table 3 also showed that the order of influence on the adsorption capacity of MB by M-SSAC was: adsorbent dosage > pH > initial MB concentration > adsorption time. The interaction between the four factors was not apparent, and the squared effect of adsorbent dosage was noticeable.

#### *Response Surface Model Analysis*

The three-dimensional response surface plots and contour plots of the effect of pH, adsorbent dosage, initial MB concentration, and adsorption time on the adsorption capacity of MB by the M-SSAC are shown in Fig. 1. It could be seen that the MB adsorption capacity increased with the increase in adsorption time and then stabilized. With the increase of the initial concentration, the MB adsorption capacity showed an increasing trend. As the adsorbent dosage of the M-SSAC increased, the MB adsorption amount gradually decreased. With the increase in pH, the adsorption capacity of M-SSAC on MB increased and then decreased. Because MB is a cationic dye, at low pH, the adsorption capacity increased as the electrostatic gravitational force between the M-SSAC and MB increased with the increase in pH [20]. At higher pH values, the electrostatic repulsion between MB and the M-SSAC increased, so the adsorption capacity increased and then decreased with increasing pH.

#### *Optimization Validation*

The optimal adsorption conditions for MB adsorption by the M-SSAC adsorbent were obtained using Design-Experts 8.0.6 software, combined with the regression model, the optimum adsorption conditions

Table 2. Experimental design and adsorption capacity analysis.

Numbers	Actual values				Coded values				Measured value Y (mg/g)	Predicted value (mg/g)
	A	B	C	D	A	B	C	D		
1	6.5	0.15	150	120	0	1	0	1	32.95	32.25
2	7.5	0.10	150	20	1	0	0	-1	41.94	40.29
3	6.5	0.10	100	20	0	0	-1	-1	34.50	33.59
4	5.5	0.10	100	70	-1	0	-1	0	28.63	28.31
5	7.5	0.10	150	120	1	0	0	1	23.63	23.03
6	6.5	0.10	100	120	0	0	-1	1	32.05	31.48
7	6.5	0.05	150	20	0	-1	0	-1	35.65	36.00
8	6.5	0.10	200	120	0	0	1	1	28.56	29.32
9	6.5	0.10	150	70	0	0	0	0	30.88	31.47
10	6.5	0.05	100	70	0	-1	-1	0	30.70	30.91
11	5.5	0.10	200	70	-1	0	1	0	26.72	27.27
12	6.5	0.10	150	70	0	0	0	0	24.95	24.95
13	5.5	0.10	150	120	-1	0	0	1	32.32	33.17
14	7.5	0.15	150	70	1	1	0	0	39.35	39.44
15	5.5	0.10	150	20	-1	0	0	-1	19.63	19.60
16	6.5	0.15	200	70	0	1	1	0	33.70	33.96
17	7.5	0.05	150	70	1	-1	0	0	31.87	32.00
18	6.5	0.10	150	70	0	0	0	0	24.51	24.87
19	5.5	0.15	150	70	-1	1	0	0	25.71	26.56
20	6.5	0.15	100	70	0	1	-1	0	17.39	17.83
21	6.5	0.05	200	70	0	-1	1	0	40.18	40.82
22	5.5	0.05	150	70	-1	-1	0	0	32.44	32.24
23	6.5	0.15	150	20	0	1	0	-1	32.33	31.80
24	6.5	0.10	150	70	0	0	0	0	26.74	26.68
25	6.5	0.10	150	70	0	0	0	0	33.16	32.22
26	6.5	0.10	200	20	0	0	1	-1	25.64	25.04
27	7.5	0.10	200	70	1	0	1	0	32.81	32.08
28	6.5	0.05	150	120	0	-1	0	1	33.05	32.28
29	6.5	0.10	150	70	0	0	0	0	24.16	23.29
30	7.5	0.10	100	70	1	0	-1	0	18.38	17.81

of the M-SSAC for MB were obtained: the pH was 6.6, the adsorbent dosage was 0.05 g, the initial MB concentration was 190 mg/L, and the adsorption time was 110 min. The capacity of MB adsorption by the M-SSAC under the optimal adsorption conditions was 42.83 mg/g. To test the reliability of the adsorption capacity obtained by the response surface method, three validation tests were carried out under optimal adsorption conditions. The results showed that the average adsorption capacity of the M-SSAC for MB was

41.96 mg/g under the optimal adsorption conditions, with an error of 1.19% from the predicted value, indicating that the optimized adsorption conditions based on the RSM were accurate and reliable.

#### Adsorption Isotherm

The initial concentration of MB was selected from 20 to 400 mg/L, the dosage of M-SSAC was 2.0 g/L, and the pH of the original MB solution was 6.6.

Table 3. Response surface model results and significance analysis.

Source	Sum of Squares	Df	Mean Square	F Value	P value (Prob>F)
Model	1048.88	14	74.92	190.91	<0.0001***
A	100.88	1	100.88	257.07	<0.0001***
B	208.26	1	208.26	530.69	<0.0001***
C	100.06	1	100.06	254.98	<0.0001***
D	70.41	1	70.41	179.41	<0.0001***
AB	0.25	1	0.25	0.63	0.4409
AC	0.04	1	0.04	0.09	0.7679
AD	0.65	1	0.65	1.65	0.2188
BC	0.33	1	0.33	0.84	0.3752
BD	0.00	1	0.00	0.00	0.9821
CD	0.28	1	0.28	0.71	0.4120
A <sup>2</sup>	512.21	1	512.21	1305.22	< 0.0001***
B <sup>2</sup>	1.93	1	1.93	4.92	0.0424*
C <sup>2</sup>	4.04	1	4.04	10.29	0.0059**
D <sup>2</sup>	1.26	1	1.26	3.20	0.0939
Residual	5.89	15	0.39		
Lack of fit	5.06	10	0.51	3.05	0.1148
Pure error	0.83	5	0.17		
Cor total	1054.77	29			

Notes: \*significant at P<0.05; \*\*significant at P<0.01; \*\*\*significant at P<0.0001.

The adsorption equilibrium was achieved by shaking the MB solution in a thermostat water bath for 120 min to investigate the effects of temperature (288, 298, 308 K) and initial MB concentration. The two adsorption isotherm equations' linear and nonlinear expressions are shown in Eq. (3) and Eq. (4), respectively.

$$q_e = \frac{q_m K_L C_e}{1 + K_L C_e} \tag{3}$$

$$q_e = K_F C_e^{\frac{1}{n}} \tag{4}$$

where  $q_e$  is the equilibrium adsorption quantity, mg/g;  $C_e$  is the equilibrium concentration of the solution, mg/L;  $q_m$  is the saturation adsorption capacity, mg/g;  $K_L$  is the Langmuir adsorption constant, L/mg;  $K_F$  is the Freundlich constant, indicating the adsorption capacity;  $n$  is the Freundlich constant, indicating the adsorption strength. When  $1/n$  is between 0 and 1, the adsorption process is easy, and when  $1/n > 1$ , the adsorption process is not easy.

Figs 2 and 3 show the adsorption isotherms of the M-SSAC on MB at different temperatures, and the related results are shown in Table 4. It could be seen that the adsorption of MB by the M-SSAC increased

gradually with the increase in temperature, which indicated that the warming was beneficial to the adsorption of MB and that the adsorption process was a heat absorption process. Compared with the Freundlich model, the Langmuir model was better fitted. The correlation coefficients  $R^2$  obtained by fitting the Langmuir model at different temperatures ranged from 0.9849 to 0.9722, indicating that the Langmuir adsorption isotherm model could better simulate the adsorption of M-SSAC on MB. The adsorption of MB by the M-SSAC occurs on the surface of the adsorbent as a single molecular layer adsorption [21]. The MB molecule is adsorbed by the M-SSAC and will be uniformly arranged at each adsorption site, and surface adsorption plays a prominent role throughout the adsorption process [22]. In addition,  $K_F$  in Freundlich model increased with adsorption temperature, that is, the adsorption capacity increased with adsorption temperature, indicating that the adsorption process was a heat absorption process.

### Adsorption Kinetics

For ease of calculation, the initial MB concentration was 200 mg/L (pH = 6.6), and the concentration of M-SSAC was 2.0 g/L. The effect of adsorption time

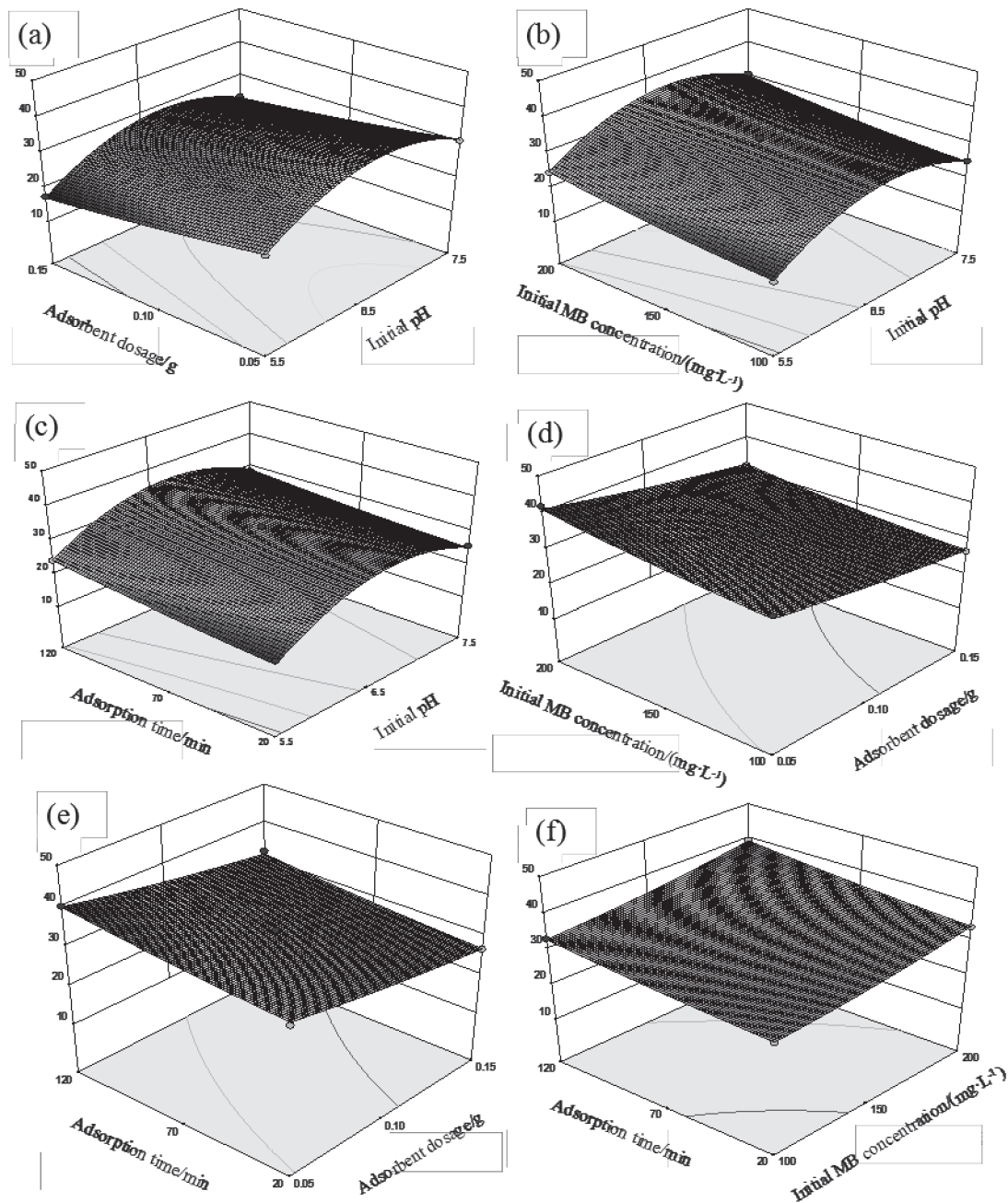


Fig. 1. Three-Dimensional Response Surface Plots and Contour Plots for the Four Influencing Factors. a) A-B, b) A-C, c) A-D, d) B-C, e) B-D, f) C-D.

on the adsorption process of MB at different temperatures was investigated. The Pseudo-first-order and Pseudo-second-order kinetic models were selected to fit the experimental data. The fitted equations are shown in Eq. (5) and Eq. (6), respectively.

$$q_t = q_e (1 - e^{-k_1 t}) \quad (5)$$

$$q_t = \frac{k_2 q_e^2 t}{1 + k_2 q_e t} \quad (6)$$

Where  $t$  is the adsorption time, min;  $q_e$  is the adsorption of M-SSAC at equilibrium, mg/g;  $q_t$  is the adsorption of M-SSAC at time  $t$ , mg/g;  $k_1$  is the rate constant for Pseudo-second-order kinetics, min<sup>-1</sup>;  $k_2$  is the rate constant of Pseudo-second-order kinetics, g/(mg·min).

The results are shown in Fig. 4, Fig. 5, and Table 5. As shown in Table 5, when the Pseudo-first-order kinetic model was fitted, although the correlation coefficients were above 0.94, the  $q_{e,cal}$  (theoretical value of  $q_e$ ) was much lower than the actual value, indicating that the Pseudo-first-order kinetic model was not suitable for

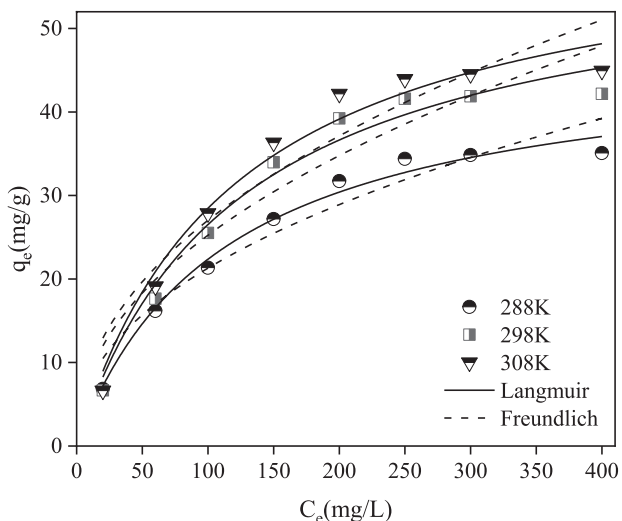


Fig. 2. Nonlinear fitted curves with isotherm models of MB by the M-SSAC.

describing the process of MB adsorption by M-SSAC. When the Pseudo-second-order kinetic model was fitted, the correlation coefficients were higher compared to the Pseudo-first-order kinetic model, basically above 0.99, indicating that chemisorption plays a decisive role in the adsorption of MB by M-SSAC, and that this adsorption process may involve valence forces between dye

molecules and soybean straw using shared or exchanged electrons [23]. In addition,  $q_{e,cal}$  is close to the measured value, indicating that the Pseudo-second-order kinetic model can well describe the adsorption process of M-SSAC on MB. The values of  $k_2$  and  $q_{e,cal}$  increased with the increase of adsorption temperature, verifying that the adsorption process is a heat absorption process.

### Adsorption Thermodynamics

Adsorption thermodynamic parameters of the M-SSAC on MB adsorption processes, such as Gibbs free energy ( $\Delta G^0$ , kJ/mol), enthalpy change ( $\Delta H^0$ , kJ/mol) and entropy change ( $\Delta S^0$ , J/(mol·K)), can be calculated from Eq. (7)~(9).

$$K_c = \frac{C_{ad}}{C_e} \tag{7}$$

$$\Delta G^0 = -RT \ln K_c \tag{8}$$

$$\Delta G^0 = \Delta H - T\Delta S \tag{9}$$

Where  $C_{ad}$  and  $C_e$  are the amount of MB in M-SSAC and solution at adsorption equilibrium (mg/g), respectively;  $R$  is the ideal gas constant, 8.314 J/(mol·K);  $T$  is the absolute temperature, K;  $K$  is the partition coefficient.

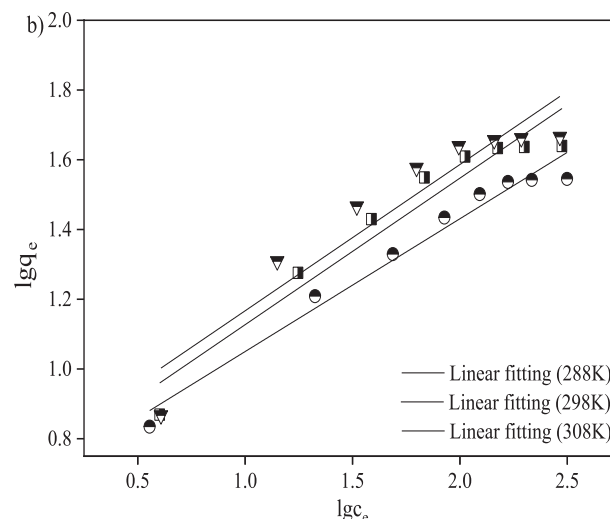
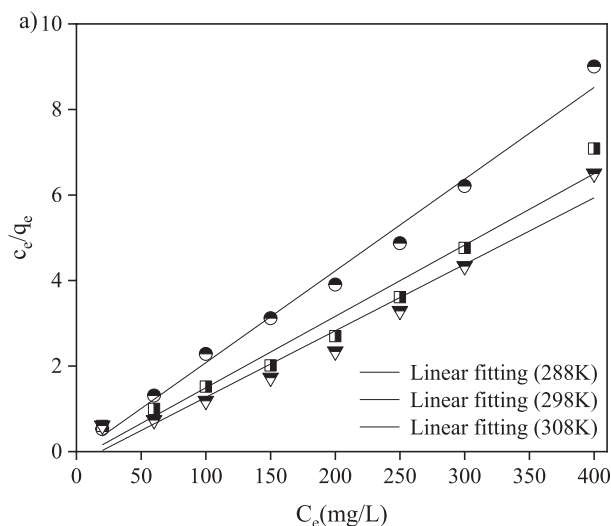


Fig. 3. Linear fitted curves with isotherm models of MB by the M-SSAC. a) Langmuir, b) Freundlich.

Table 4. Parameters of isotherm model at different temperatures.

Temperature/K	Langmuir			Freundlich		
	$Q_m$ (mg/g)	$K_L$ (L/mg)	$R^2$	$K_F$	n	$R^2$
288	47.45	0.0089	0.9849	2.80	0.4407	0.9248
298	59.29	0.0081	0.9728	3.00	0.4624	0.8976
308	62.62	0.0083	0.9722	3.27	0.4586	0.8919

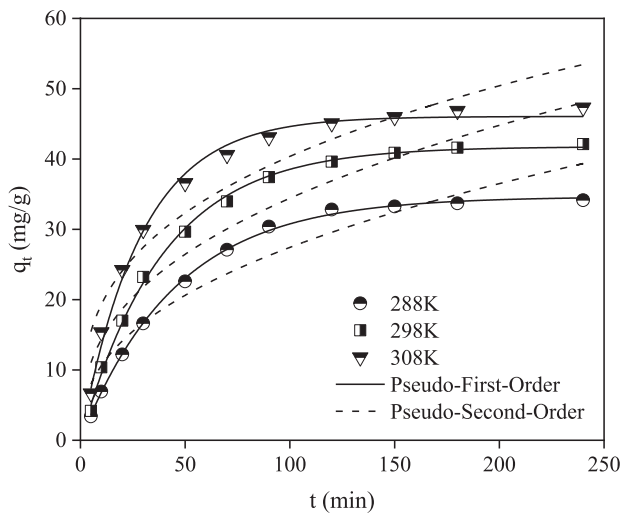


Fig. 4. Nonlinear fitted curve with dynamic adsorption models of MB by the M-SSAC.

The results of the thermodynamically relevant parameters are calculated as shown in Table 6. The value of  $\Delta G < 0$ , indicating that the process of MB adsorption by M-SSAC proceeds spontaneously. As the temperature increased from 288 K to 298 K and 308 K,  $\Delta G^0$  increased from -11.28 kJ/mol to -12.26 kJ/mol and -12.89 kJ/mol accordingly, indicating that increasing

Table 6. Thermodynamic parameters for the adsorption of MB by the M-SSAC.

Temperature (k)	$\Delta G^0$ (kJ/mol)	$\Delta H^0$ (kJ/mol)	$\Delta S^0$ (kJ·mol <sup>-1</sup> ·K <sup>-1</sup> )
288	-11.28	10.53	0.8085
298	-12.26		
308	-12.89		

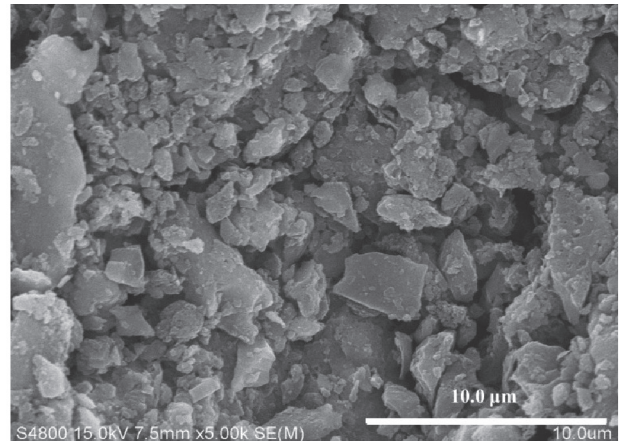


Fig. 6. Scanning electron micrographs of the M-SSAC.

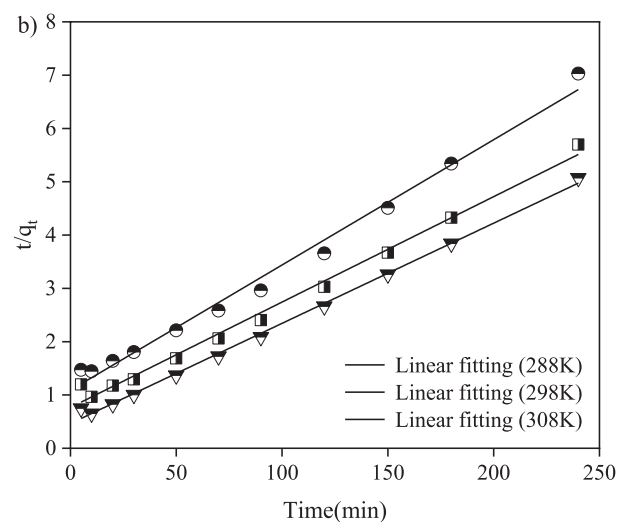
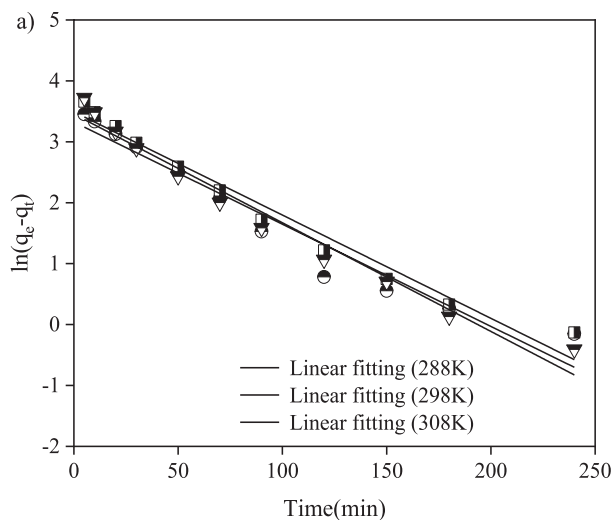


Fig. 5. Linear fitted curve with dynamic adsorption models of MB by the M-SSAC a) Pseudo-first-order, b) Pseudo-second-order.

Table 5. Adsorption kinetic parameters of MB by M-SSAC.

Temperature /K	Pseudo-first-order			Pseudo-second-order		
	$q_{e,cal}$ (mg/g)	$k_1$ (min <sup>-1</sup> )	$R^2$	$q_{e,cal}$ (mg/g)	$k_2$ (g·mg <sup>-1</sup> ·min <sup>-1</sup> )	$R^2$
288	27.78	0.0168	0.9465	42.55	0.00051	0.9897
298	32.87	0.0170	0.9722	50.56	0.00056	0.9906
308	31.67	0.0178	0.9681	53.22	0.00076	0.9969

the temperature favored the adsorption process [24]. The value of  $\Delta H$  was 10.53 kJ/mol, indicating that the adsorption process absorbed heat and increasing the temperature favored the adsorption, which is consistent with the adsorption isotherm study. The value of  $\Delta S$  was 0.8085 kJ/(mol·K), indicating an increase in the degree of freedom of the solid-liquid surface during the adsorption of MB by the M-SSAC [25]. The above results indicated that the adsorption of MB by the M-SSAC proceeds spontaneously, accompanied by an increase in the energy of the system.

### SEM Analysis

The surface of the M-SSAC was found to be highly microporous and fragmented in texture in combination with SEM image (Fig. 6). From the morphology of the char particles in Figure 6, it was found that the char particles showed a fragmented fracture pattern and formed depressions inside. This is due to the catalytic, oxidizing and dehydrating functions of sodium hypochlorite, which can promote the pyrolysis of cellulose during the carbonization process and escape in the form of CO and water vapor, resulting in the formation of fragmented fissures [26]. This asymmetric surface and open pore structure gives M-SSACA a rich specific surface area.

### Conclusions

(1) The results of the response surface optimization showed that the significant factors affecting the adsorption capacity of the M-SSAC for MB were adsorbent dosage > pH > initial MB concentration > adsorption time, and the values of pH and initial MB concentration were close to each other. The optimal adsorption conditions for the adsorption capacity of M-SSAC on MB predicted by the response surface method were: the pH was 6.6, the adsorbent dosage was 0.05 g, the initial MB concentration was 190 mg/L, and the adsorption time was 110 min. Under these conditions, the average adsorption capacity of the M-SSAC on MB was 41.96 mg/g.

(2) The Langmuir model was more suitable than the Freundlich model for simulating the adsorption equilibrium test data at three different temperatures of 288 K, 298 K, and 308 K. At 308 K, the maximum adsorption capacity calculated by the Langmuir adsorption isotherm model was 62.62 mg/g.

(3) The kinetics of MB adsorption by the M-SSAC adsorbent was consistent with the Pseudo-second-order kinetic model, and the thermodynamic calculations indicated that the adsorption reaction of the M-SSAC on MB was spontaneous and the adsorption process was heat absorption.

(4) The current research often focuses on the adsorption of MB by the adsorbent. Further research should deepen the material analysis and adsorption

mechanism analysis of the M-SSAC on the one hand and consider the influence of complex components on the adsorption effect in the actual wastewater on the other hand.

### Acknowledgments

This work was supported by the funding provided by the Science and Technology Planning Project of Changzhou (CJ20210054).

### Conflict of Interest

The authors declare no conflict of interest.

### References

- BOUYAHIA C., RAHMANI M., BENSEMLALI M., EL HAJJAJI S., SLAOUI M., BENCHEIKH I., AZOULAY K., LABJAR N. Influence of extraction techniques on the adsorption capacity of methylene blue on sawdust: Optimization by full factorial design. *Materials Science for Energy Technologies*, **6**, 114, **2023**.
- MOEINIAN K., MEHDINIA S.M. Removing Methylene Blue from Aqueous Solutions Using Rice Husk Silica Adsorbent. *Polish Journal of Environmental Studies*, **28** (4), 2281, **2019**.
- ZHANG H., PENG B., LIU Q., WU C., LI Z. Preparation of porous biochar from heavy bio-oil for adsorption of methylene blue in wastewater. *Fuel Processing Technology*, **238**, 107485, **2022**.
- SINGH S., YADAWA Y., RANJAN A. Enhanced adsorption of methylene blue by mixed-phase bismuth ferrite prepared by non-aqueous sol-gel route. *Journal of Environmental Chemical Engineering*, **11** (1), 109229, **2023**.
- MARZBAN N., MOHEB A., FILONENKO S., HOSSEINI S.H., NOURI M.J., LIBRA J.A., FARRU G. Intelligent modeling and experimental study on methylene blue adsorption by sodium alginate-kaolin beads. *International Journal of Biological Macromolecules*, **186**, 79, **2021**.
- OLADOYE P.O., AJIBOYE T.O., OMOTOLA E.O., OYEWOLA O.J. Methylene blue dye: Toxicity and potential elimination technology from wastewater. *Results in Engineering*, **16**, 100678, **2022**.
- LI Q., LI Y., MA X., DU Q., SUI K., WANG D., WANG C., LI H., XIA Y. Filtration and adsorption properties of porous calcium alginate membrane for methylene blue removal from water. *Chemical Engineering Journal*, **316**, 623, **2017**.
- RANJBARI A., KIM J., KIM J.H., YU J., DEMEESTERE K., HEYNDERICKX P.M. Enhancement of commercial ZnO adsorption and photocatalytic degradation capacity of methylene blue by oxygen vacancy modification: Kinetic study. *Catalysis Today*, **2022**.
- TEIXEIRA Y.N., de PAULA FILHO F.J., BACURAU V.P., MENEZES J.M.C., ZHONG FAN A., MELO R.P.F. Removal of Methylene Blue from a synthetic effluent by ionic flocculation. *Heliyon*, **8** (10), e10868, **2022**.
- MASHKOOR F., NASAR A. Magsorbents: Potential candidates in wastewater treatment technology

- A review on the removal of methylene blue dye. *Journal of Magnetism and Magnetic Materials*, **500**, 166408, **2020**.
11. RAFATULLAH M., SULAIMAN O., HASHIM R., AHMAD A. Adsorption of methylene blue on low-cost adsorbents: A review. *Journal of Hazardous Materials*, **177** (1), 70, **2010**.
  12. SANTOSO E., EDIATI R., KUSUMAWATI Y., BAHRUJI H., SULISTIONO D. O., PRASETYOKO D. Review on recent advances of carbon based adsorbent for methylene blue removal from waste water. *Materials Today Chemistry*, **16**, 100233, **2020**.
  13. DOLAS H. Activated carbon synthesis and methylene blue adsorption from pepper stem using microwave assisted impregnation method: Isotherm and kinetics. *Journal of King Saud University - Science*, **35** (3), 102559, **2023**.
  14. FATIMAH I., FADILLAH G., AYU REDNASARI R., WAHYUNINGSIH S. Green reduction of graphene oxide using *Annona muricata* leaves extract for adsorption of methylene blue. *Inorganic Chemistry Communications*, **146**, 110144, **2022**.
  15. JIAO S., YAO Y., ZHANG J., ZHANG L., LI C., ZHANG H., ZHAO X., CHEN H., JIANG J. Nano-flower-like porous carbon derived from soybean straw for efficient N-S co-doped supercapacitors by coupling in-situ heteroatom doping with green activation method. *Applied Surface Science*, **615**, 156365, **2023**.
  16. WANG Z., HOU X., WANG Y., COLLINS E., DUAN P. Hydrothermal liquefaction of soybean straw: Effect of steam explosion pretreatment and reaction media. *Fuel*, **339**, 127418, **2023**.
  17. JIAO S., ZHANG L., LI C., ZHANG H., ZHANG J., LI P., TAO Y., ZHAO X., CHEN H., JIANG J. Efficient construction of a carbon-based symmetric supercapacitor from soybean straw by coupling multi-stage carbonization and mild activation. *Industrial Crops and Products*, **183**, 114906, **2022**.
  18. ADHIKARY S.K., ASHISH D.K., RUDŽIONIS }. A review on sustainable use of agricultural straw and husk biomass ashes: Transitioning towards low carbon economy. *Science of the Total Environment*, **838**, 156407, **2022**.
  19. MIAO Q., TANG Y., XU J., LIU X., XIAO L., CHEN Q. Activated carbon prepared from soybean straw for phenol adsorption. *Journal of the Taiwan Institute of Chemical Engineers*, **44** (3), 458, **2013**.
  20. de ARAÚJO L.F.B., MAZZETTO S.E., LOMONACO D., AVELINO F. Unraveling the adsorption mechanism of methylene blue onto selective pH precipitated Kraft lignins: Kinetic, equilibrium and thermodynamic aspects. *International Journal of Biological Macromolecules*, **220**, 1267, **2022**.
  21. XU Q., LIU T., LI L., LIU B., WANG X., ZHANG S., LI L., WANG B., ZIMMERMAN A.R., GAO B. Hydrothermal carbonization of distillers grains with clay minerals for enhanced adsorption of phosphate and methylene blue. *Bioresource Technology*, **340**, 125725, **2021**.
  22. LI H., BUDARIN V. L., CLARK J.H., NORTH M., WU X. Rapid and efficient adsorption of methylene blue dye from aqueous solution by hierarchically porous, activated starbons®: Mechanism and porosity dependence. *Journal of Hazardous Materials*, **436**, 129174, **2022**.
  23. ZHANG Y., SHEN B., SAJJAD AHMAD M., ZHOU W., KHALID R.R., IBRAHIM M., BOKHARI A. A three-dimensional active biochar for sintering in steel industry and remove methylene blue by synergistic activation of  $H_3PO_4$  and  $ZnCl_2$ . *Fuel*, **336**, 127079, **2023**.
  24. LIU S., LI J., XU S., WANG M., ZHANG Y., XUE X. A modified method for enhancing adsorption capability of banana pseudostem biochar towards methylene blue at low temperature. *Bioresource Technology*, **282**, 48, **2019**.
  25. XIONG Y.Y., LI J.Q., GONG L.L., FENG X.F., MENG L.N., ZHANG L., MENG P.P., LUO M.B., LUO F. Using MOF-74 for  $Hg^{2+}$  removal from ultra-low concentration aqueous solution. *Journal of Solid State Chemistry*, **246**, 16, **2017**.
  26. MAO B., WANG Y., ZHAO T., ZHAO Q., SAN Y., XIAO S. Response of carbon, nitrogen and phosphorus concentration and stoichiometry of plants and soils during a soybean growth season to O<sub>3</sub> stress and straw return in Northeast China. *Science of the Total Environment*, **822**, 153573, **2022**.